Applied Catalysis B: Environmental 204 (2017) 250–259

Contents lists available at ScienceDirect

Applied Catalysis B: Environmental

journal homepage: www.elsevier.com/locate/apcatb

Study on the photocatalytic mechanism and detoxicity of gemfibrozil by a sunlight-driven TiO_2/carbon dots photocatalyst: The significant roles of reactive oxygen species

Ping Chen[a], Fengliang Wang[a], Zhi-Feng Chen[a], Qianxin Zhang[a], Yuehan Su[a], Lingzhi Shen[a], Kun Yao[a], Yang Liu[b], Zongwei Cai[c], Wenying Lv[a], Guoguang Liu[a,*]

[a] School of Environmental Science and Engineering, Institute of Environmental Health and Pollution Control, Guangdong University of Technology, Guangzhou 510006, China
[b] Faculty of Environmental and Biological Engineering, Guangdong University of Petrochemical Technology, Maoming 525000, China
[c] State Key Laboratory of Environmental and Biological Analysis, Department of Chemistry, Hong Kong Baptist University, Hong Kong, China

ARTICLE INFO

Article history:
Received 1 September 2016
Received in revised form
12 November 2016
Accepted 19 November 2016
Available online 20 November 2016

Keywords:
Gemfibrozil
TiO_2
Carbon dots
Reactive oxygen species
Detoxicity

ABSTRACT

An environmentally friendly and sunlight-driven photocatalyst is thought to be a promising alternative to conventional water treatment technology. In this study, carbon dots (C-Dots), a newly discovered material with the ability to upconvert light, were decorated to TiO_2 via a facile hydrothermal-calcination synthesis approach. Under simulated sunlight irradiation, a very low C-Dots content of 5.0 wt% resulted in a 2.3 times faster reaction rate for gemfibrozil (GEM) photodegradation than pristine TiO_2. Oxidative species, particularly •OH, were the most important reactive species mediating the photocatalytic degradation of GEM. A notable observation was the higher formation rates of •OH in the TiO_2/C-Dots system than in pristine TiO_2, which was determined via electron spin resonance spectroscopy. Frontier electron density calculations and mass spectrometry were used to verify that the major degradation pathways of GEM contained •OH addition, H abstraction and $O_2^{\bullet-}$ attack. The acute toxicity of the treated solution at two trophic levels first increased slowly and then decreased rapidly as the total organic carbon decreased during photocatalytic degradation. Compared to traditional advanced oxidation processes, TiO_2/C-Dots photocatalytic technology could reduce the generation of toxic by-products. These results highlight the potential application of sustainable sunlight-driven photocatalyst in water purification.

1. Introduction

Gemfibrozil (GEM) is a drug for regulating blood lipid content that is widely used throughout the world. Its octanol/water partition coefficient and acidity coefficient was 4.77 and 4.70, respectively (Supplementary material, Table S1). After application, GEM enters into wastewater treatment plants and then reaches the receiving environment. GEM has been found in influent, effluent and freshwater at concentrations that range from 0.07 to 0.51 $\mu g\,l^{-1}$ [1,2]. This can be attributed to the incomplete removal of GEM during wastewater treatment [3]. Since the presence of GEM may pose potential adverse effects on non-target organisms [2], it is necessary to improve the elimination efficiency of GEM by water treatment techniques.

As we known, GEM is not readily biodegradable. Chemical oxidation may be an alternative tool for the removal of GEM. Advanced oxidation processes (AOPs), including ozonation, ray irradiation, chlorination, and UV irradiation, have been conducted to remove various pharmaceuticals and personal care products (PPCPs) from wastewater [4,5]. Among these AOPs, photocatalysis is quite effective for achieving one-pot removal under sunlight irradiation [6–8]. In addition, this technique requires none of the additional auxiliary oxidation agents (e.g., hydrogen peroxide), and the photocatalytic materials can be reused without complex processes. Therefore, a key issue is to find an appropriate photocatalyst for the effective degradation of GEM under solar irradiation.

TiO_2, as a promising photocatalyst, is widely applied to wastewater purification due to its superior photocatalytic oxidation ability and stable and nontoxic characteristics [9,10]. However, TiO_2 photocatalyst is exclusively activated with UV light ($\lambda \leq 380$ nm) [11].

* Corresponding author at: School of Environmental Science and Engineering, Guangdong University of Technology, No. 100 Waihuan Xi Road, Guangzhou Higher Education Mega Center, Guangzhou 510006, China.
E-mail address: liugg615@163.com (G. Liu).

http://dx.doi.org/10.1016/j.apcatb.2016.11.040
0926-3373/

The photocatalytic activity of TiO_2 under natural solar irradiation is largely limited. Thus, it is highly desirable to design and seek efficient photocatalysts for the treatment of PPCPs under sunlight irradiation [12,13]. Carbon dots (C-Dots) are a type of new quantum dot with unique optical and electronic properties. In recent years, they have been utilized as modifying materials to enhance the photocatalytic activity of traditional photocatalysts under simulated sunlight irradiation [14–18]. C-Dots have been demonstrated to possess excellent upconversion photoluminescence (UCPL). That is, lower-energy light (visible or near-infrared light from 500 to 1000 nm) can be converted to higher-energy light (ultraviolet or visible light from 325 to 425 nm) via the multiple photon absorption property of C-Dots [19,20]. This implies that the upconversion function of C-Dots enables the visible and near-infrared spectrum of sunlight to be utilized, resulting in an enhancement of photocatalytic efficiency [21,22]. Therefore, C-Dots were chosen to couple with TiO_2 for the enhancement of photocatalytic activity.

Previous studies regarding the photocatalytic degradation of dyes (such as MO, RhB and methyl blue) and hydrogen storage with C-Dots-based TiO_2 materials have been performed over the past few years [11,18,23]. However, the photocatalytic effect of C-Dots embedded in TiO_2 on the degradation of PPCPs has not been reported, particularly for GEM [2]. During the process of photocatalysis, reactive species (RSs) including superoxide anion radicals ($O_2^{\bullet -}$) and hydroxyl radicals ($^{\bullet}OH$) can be generated. Using electron spin resonance (ESR) to determine the most important RSs mediating the mechanism of photocatalytic degradation is a better approach than methods that employ free radical quenching tests. In addition, quantum chemical calculation was employed to further verify the degradation mechanisms [24,25].

The objectives of this work were: (1) to synthesize a sunlight-driven hybrid photocatalyst comprised of C-Dots and TiO_2 using a facile hydrothermal-calcination synthesis approach; (2) to determine the photocatalytic activity of this hybrid photocatalyst for the degradation of GEM under simulated sunlight irradiation; (3) to elucidate the degradation pathways of GEM by identifying the corresponding degradation by-products; (4) to evaluate the change of toxicity during the photocatalytic degradation of GEM; (5) to clarify the effects of specific free radicals on the photocatalytic kinetics and mechanism.

2. Experimental

2.1. Materials and reagents

GEM, 5-(2,5-dimethyl-phenoxy)-2,2-dimethyl-pentanoic acid (98% purity), was purchased from TCI Reagent Co. Ltd. (Shanghai, China). Dimethyl pyridine N-oxide (DMPO), was purchased from Sigma-Aldrich. HPLC-grade reagents (acetonitrile, methanol, etc.) were obtained from U.S. ACS Enke Chemistry Co. Ltd. (Guangzhou, China). Other reagents (e.g., $TiCl_4$, ammonium nitrate, citric acid, urea, acetic acid, sulfuric acid, sodium hydroxide and isopropanol) were of analytical grade and used without further purification. Ultra-pure water from a Milli-Q apparatus (Smart2 Pure ultrapure water/water system integration, TKA, Germany) was used in the preparation of all aqueous solutions.

2.2. Preparation and characterization methods

2.2.1. Preparation of TiO_2 nanoparticles

A measured volume (5 ml) of $TiCl_4$ was mixed with 15 ml of hydrochloric acid solution (pH = 1.5–2.0) in a single round neck flask, and stirred for 20 min. To the mixed solution, 1.2 times the $TiCl_4$ (molar ratio) of urea and 7.0 times the $TiCl_4$ (molar ratio) of ammonium nitrate was added and the solution was mixed by magnetic stirring for 10 min and transferred to a Teflon autoclave for 30 min at 160 °C. Then, the solution was transferred to a muffle furnace for 30 min at 400 °C, washed several times with absolute ethanol and dried under vacuum to obtain TiO_2 nanoparticles.

2.2.2. Preparation of C-Dots

C-Dots were prepared by the hydrothermal method, and modified according to the procedure given in a previous report [26]. Briefly, a weighed quantity (3.0 g) of citric acid and (3.0 g) of urea were mixed with 10 ml of ultrapure water, which was placed into a Teflon autoclave for 5 h at 180 °C. After it was cooled to room temperature, a brown water solution was obtained. Large particles were removed by centrifugation at 10000 r/min for 15 min, then the remaining solution was transferred to the vacuum drier for 3 h at 80 °C to obtain a brownish black solid (C-Dots).

2.2.3. Deposition of C-Dots on TiO_2

Different amounts of TiO_2 and C-Dots were accurately weighed. The mixed powder was dispersed in 20 ml of ethanol and 10 ml of ultrapure water in an alumina crucible, and stirred to dry the moisture in a fuming cupboard. Then, the mixture was transferred to a muffle furnace for 3 h at 300 °C. After the reaction, the products were cooled to room temperature and washed several times with distilled water and ethanol. Afterwards, the substance was dried under vacuum at room temperature for 24 h to obtain the TiO_2 functionalized with C-Dots, which we denote as a functional TiO_2/C-Dots photocatalyst (light gray powder).

2.2.4. Characterization methods

The morphology of the photocatalyst was determined by field transmission micrographs produced from a JEOL JEM-2100F transmission electron microscope (TEM) operating at an acceleration voltage of 200 kV. For TEM analysis, the photocatalysts were dissolved in ethanol and prepared by sonication to achieve uniform dispersion, subsequently a few drops of the mixture were transferred by a pipette onto a carbon-coated copper grid. The phase compositions and x-ray diffraction (XRD) patterns were collected on a Rigaku Ultima III diffractometer by using Cu ka radiation ($\lambda = 1.5406$ Å), with a scanned area of $2\theta = 10–70°$. The presence of O, Ti and C in the composites was analyzed using x-ray photoelectron spectroscopy (XPS, PHI Quantera 2X) with non-monochromated Mg-Kα radiation as the excitation source. Fourier transform infrared spectra (FT-IR) were recorded on a Thermofisher Nicolet 6700 spectrometer to analyze the functional groups of samples. Quantitative analysis of photocatalyst surface elements were performed using energy disperse spectroscopy (EDS) recorded using a HORIBA EX-250 analyzer. The upconverted PL spectra of C-Dots were detected by a Hitachi F7000 fluorescence spectrometer (Japan). The spectra of GEM and TiO_2/C-Dots suspensions were scanned using a UV–vis spectrophotometer (UV-2100, Beijing Rayleigh) through a quartz cuvette (optical path length 1.0 cm), and the pH of the solutions was measured with a dual-star pH/ISE benchtop pH meter (Thermo). To determine the changes of mineralization during photocatalysis, total organic carbon (TOC) was measured by a TOC-VCPH analyzer (Shimadzu). Each sample was detected three times and a final TOC value was averaged in the analysis over the three measurements.

2.3. Photocatalytic degradation tests

2.3.1. Photocatalytic activity

Photocatalytic activity experiments were performed on equipment that had a hollow cylindrical quartz tube photoreactor (XPA-7, Nanjing XUJ Co. Ltd.) (Fig. S1). The light source was provided by a 350 W long-arc Xe lamp with broad spectral energy distribution ($200\ nm \leq \lambda \leq 1200\ nm$) (Fig. S2). The photoreaction

vessels included pyrex tubes (filtered light $\lambda < 290$ nm, to simulate sunlight irradiation) and quartz tubes (filtered light $\lambda \leq 200$ nm), which were placed vertically outside a double-walled quartz cooling jacket. Prior to illumination, the appropriate photocatalyst was added into the stock solution and the suspension was magnetically stirred in the dark for 30 min. This was to ensure that the adsorption/desorption equilibrium of GEM on the surface of the nano-photocatalyst had been reached. The reaction solution of GEM and other additives were stirred by a magnetic stirrer during the experiments to maintain homogeneity in the reaction vessels. For the kinetic, by-products and toxicity tests, the pyrex tubes (filtered light $\lambda < 290$ nm, to simulate sunlight irradiation) were selected as the reaction vessels. For the catalyst mechanism tests, three experiments were conducted as follows: (1) in the quartz tubes (filtered light $\lambda \leq 200$ nm) with 350 W long-arc Xe lamp irradiation; (2) in the pyrex tubes with 350 W long-arc Xe lamp irradiation; (3) in the pyrex tubes with the irradiation of 350 W long-arc Xe lamp equipped with ultraviolet cutoff filters (filtered light $\lambda < 420$ nm). At given time intervals, 3 ml of the reaction solution was collected and filtered through 0.22 μm Millipore filters to remove the nano-photocatalyst for determination of residual GEM. The detailed analytical method of GEM analysis is given in the Text S1. Three replicates were carried out for each test.

2.3.2. Identification of photocatalytic by-products

To elucidate the mechanism of the GEM reaction, the intermediate products were also investigated in this study. GEM and TiO_2/C-Dots suspension solutions were prepared for the photocatalytic experiment, then filtered by a membrane syringe filter and concentrated in a rotary evaporator (RE-5299, YU HUA INSTRUMENT) to 1.2 ml and transferred to a sample vial for characterization by HPLC/MS/MS (Agilent Technologies, USA). Separation of intermediate products was accomplished using an Agilent SB-C18 column (5 μm, 4.6 × 150 mm). Mass spectrometry analysis was conducted in negative mode using an electrospray ionization (ESI) source. The optimized parameters were as follows: fragmentor of 125 V, capillary voltage of 3.5 kV, desolvation gas (nitrogen, P99.99%) flow of 10 l min^{-1}, nebulizer pressure of 40 psi, temperature of 350 °C, scan range of *m*/*z* 100–600 and argon (P99.99%) was used as collision gas.

After the extraction by dichloromethane, the intermediate by-products were also identified by GC/MS (Agilent 6890-GC/5973i-MS) analyses. A DB-5 MS capillary column (30 m length × 0.25 mm × 0.25 μm) was used for GC separation. The GC equipments were operated in a temperature programmed mode with an initial temperature of 60 °C, subsequently ramped to 280 °C with 10 °C/min rate. Electronimpact (EI) mass spectra were scanned from 0 to 300*m*/*z*. Helium was used as the carrier gas.

2.3.3. Determination of RSs during photocatalytic degradation

ESR signals of radicals spin-trapped by DMPO were measured for detecting •OH using a Bruker A200-9.5/12 spectrometer (Germany) after simulated sunlight irradiation of the suspension (0.05 g l^{-1} catalyst, 50 mM DMPO in water) at different time intervals. Before application, DMPO was distilled and stored at −15 °C. The detections of •OH were conducted by the following ESR conditions: microwave frequency of 20 mW, sweep width of 100 Gs, sweep time of 41.96 s, modulation amplitude of 1 Gs, and center field of 3517 Gs. Due to the trace generation of $O_2^{\bullet -}$ in the present study, a more sensitive Bruker model ESR JES-FA200 spectrometer by using the DMPO in methanol (for $O_2^{\bullet -}$) was conducted. ESR conditions for the detection of $O_2^{\bullet -}$: Microwave frequency of 9053.8 MHz, sweep width of 5 mT, sweep time of 1.0 min, time constant of 0.03 s, and center field of 323.1 mT.

2.4. Calculation of frontier electron density

To further verify the degradation by-products, b3lyp/6-311+g (d, p), possessing an optimal conformation with a minimum energy obtained in the Gaussian 09 program, was used to calculate the molecular orbitals of GEM. This meant that the frontier electron densities (FEDs) of the highest occupied molecular orbital (HOMO), the lowest unoccupied molecular orbital (LUMO), and point charges were calculated. Values of the point charges were used to predict the reaction sites for H atom abstraction by •OH or $O_2^{\bullet -}$ nucleophilic attack, whereas ($FED^2_{HOMO} + FED^2_{LUMO}$) values were determined for •OH addition positions.

2.5. Risk assessment

Vibrio fischeri (*V. fischeri*) was used to measure the change of toxicity according to the Water Quality-Determination of the Acute Toxicity-Luminescent Bacteria Test (GB/T15441-1995) and another toxicity test was conducted using the aquatic organism *Daphnia magna* (*D. magna*) following the guidance of OECD (1981) [27]. The ECOSAR program (ECOSAR, 2013) was performed to predict the acute and chronic toxicities of GEM and its transformation by-products on fish, Daphnia and green algae [28]. The detailed information is provided in Text S1.

2.6. Data processing

The Gaussian 09 program at the b3lyp/6-311+g (d, p) level was used for data processing.

3. Results and discussion

3.1. Characterization of the TiO_2/C-Dots composites

In the present experiment, C-Dots with upconversion function were successfully prepared. They could be excited by long-wavelength light (from 500 to 900 nm) and the upconverted emission was located in the range of 350–650 nm (Fig. 1A). The results suggest that the visible and near infrared emission wavelengths can be converted to higher energy short wavelengths through the C-Dots. TEM images show that the small particles on the surface of TiO_2 are C-Dot nanoparticles, which are bound closely with TiO_2 and virtually no free C-Dots are observed (Figs. 1 B, C and S3).

According to the results of XRD, the characteristic diffraction lines of the TiO_2/C-Dots composites are similar to TiO_2 nanoparticles, indicating very little change in the phase of TiO_2 in the TiO_2/C-Dots composites (Fig. S4). The FT-IR spectra of the TiO_2/C-Dots composites show some new functional groups. This could be attributed to the reaction between C-Dots and TiO_2 (Fig. 1D). The XPS patterns illustrate the presence of carbon-oxygen bonds in the TiO_2/C-Dots composites (Fig. S5) in accordance with the results of the FT-IR spectra, indicating that the TiO_2/C-Dots composites are constructed through the formation of C═O and C—OH bonds originating from the surfaces of the C-Dots and TiO_2. Additional detailed information regarding the characterization of the TiO_2/C-Dots composites is provided in Text S2. The characterization results declare the successfully preparation of TiO_2/C-Dots composites, which could be potentially used in the degradation of GEM.

3.2. Photocatalytic degradation of GEM

Pyrex glasses were used to filter the UVC waveband (200–275 nm) and a portion of the UVB waveband (275–290 nm) in the present experiment. As shown in Fig. S2, the spectral energy distribution of the xenon lamp and the sunlight spectrum is very

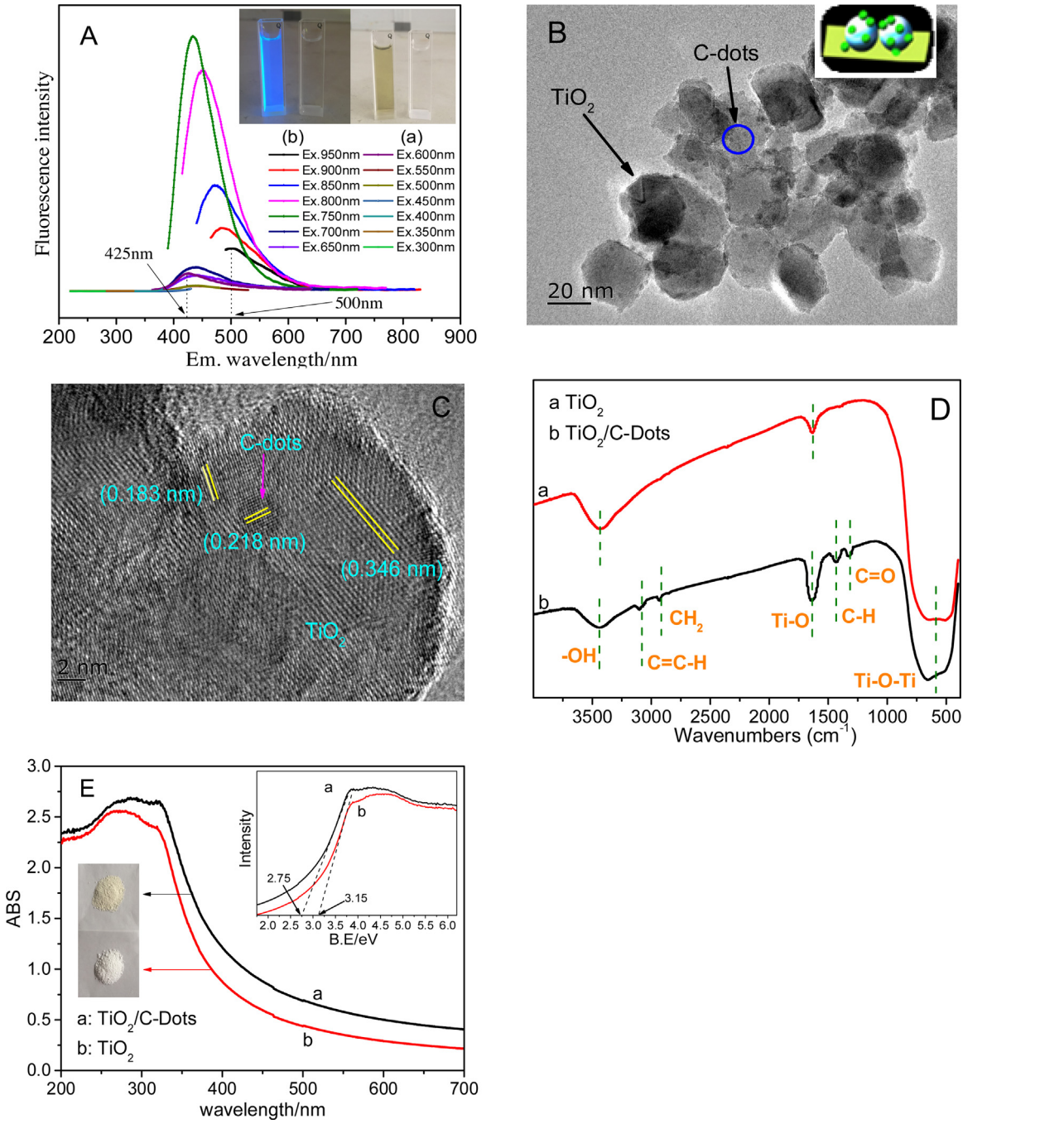

Fig. 1. (A) Upconverted PL spectra of C-Dots, inset: C-Dots dispersed in water illuminated under (a) white light and (b) UV light (excitation wavelength at 365 nm); (B) TEM images of the prepared TiO_2/C-Dots, blue circle shows the positions of C-Dots, inset: schematic illustration of the TiO_2/C-Dots composites; (C) HRTEM images of the prepared TiO_2/C-Dots; (D) FTIR spectra of (a) TiO_2 and (b) TiO_2/C-Dots composites and (E) UV–vis spectra of the TiO_2 and the TiO_2/C-Dots composites (5.0 wt%), the photographs of (a) TiO_2/C-Dots and (b) TiO_2, inset: Band gap of TiO_2 nanoparticles and the TiO_2/C-Dots composites. (For interpretation of the references to color in this figure legend, the reader is referred to the web version of this article.)

Table 1
Degradation rate constants of GEM with different conditions under simulated sunlight irradiation, [Catalyst] = 0.05 g l^{-1}; [GEM] = 2 mg l^{-1}; pH = 7.0.

Different conditions	Kinetic equation(x/min)	(k)/min^{-1}	$t_{1/2}$/min	Correlation coefficient/R^2
photolysis	$\ln(C/C_0) = -(4.6 \pm 0.17) \times 10^{-3}x$	0.0046	150.68	0.9856
hydrolysis[a]	$\ln(C/C_0) = -(2.1 \pm 0.09) \times 10^{-3}x$	0.0021	330.07	0.9582
0 wt%	$\ln(C/C_0) = -(43.6 \pm 2.1) \times 10^{-3}x$	0.0436	15.90	0.9713
1.0 wt%	$\ln(C/C_0) = -(62.7 \pm 1.8) \times 10^{-3}x$	0.0627	11.05	0.9687
5.0 wt%	$\ln(C/C_0) = -(101 \pm 3.7) \times 10^{-3}x$	0.101	6.89	0.9874
10.0 wt%	$\ln(C/C_0) = -(72.8 \pm 1.4) \times 10^{-3}x$	0.0728	9.52	0.9924
20.0 wt%	$\ln(C/C_0) = -(52.3 \pm 2.3) \times 10^{-3}x$	0.0523	13.25	0.9674

[a] The effect of hydrolysis means the effect in the condition of dark control.

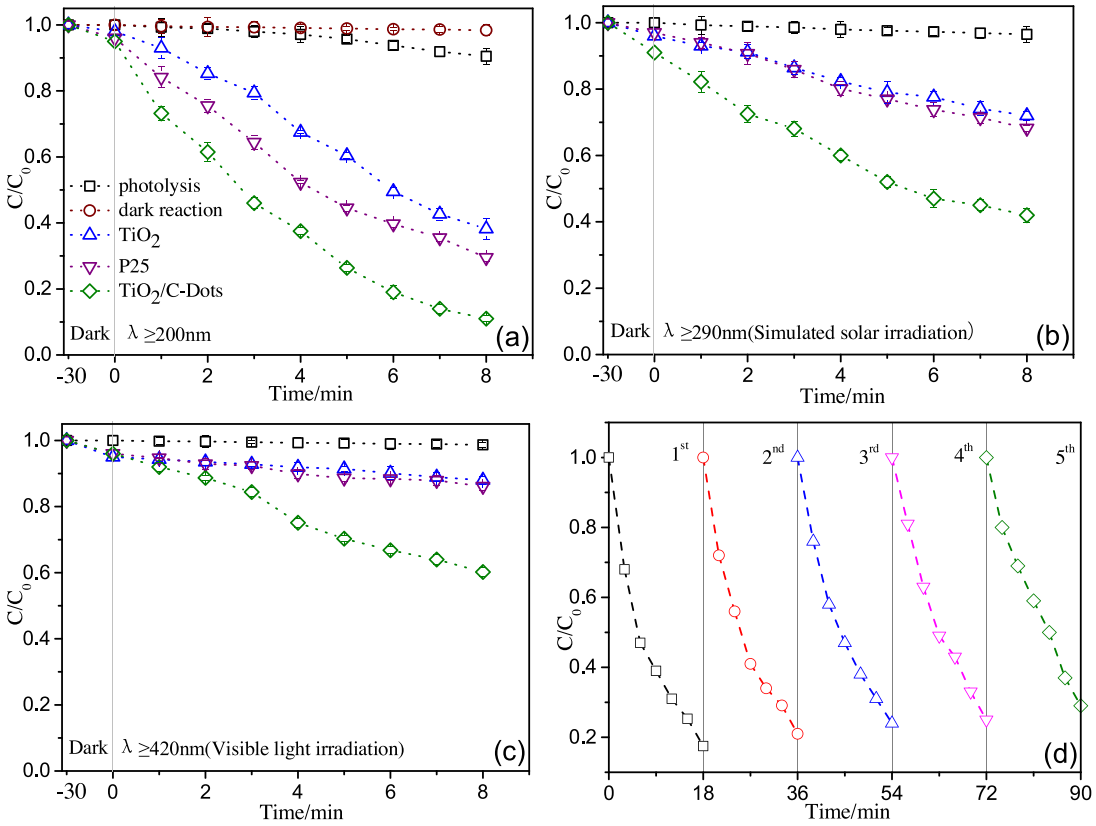

Fig. 2. Photocatalytic degradation of GEM in the presence of TiO_2 nanoparticles, P25 and TiO_2/C-Dots composites (5.0 wt%) under (a) full wavelength, (b) simulated sunlight, (c) visible light irradiation and (d) photocatalytic degradation activity after five cycles of TiO_2/C-Dots composites (5.0 wt%) under simulated sunlight irradiation.

similar. The degradation rates under different conditions are shown in Table 1. The results show that the half-life of GEM is more than 300 min in the absence of simulated sunlight irradiation, suggesting minimal effects of hydrolysis in the present study. During the adsorption/desorption equilibrium of GEM on the surface of TiO_2, P25 and TiO_2/C-Dots nanoparticles, the removal percentages of GEM via adsorption were 2.1%, 3.7% and 5.0%, respectively (Fig. 2b). Therefore, the photocatalyst adsorption of GEM is not the primary mechanism in this study.

Table 1 shows the photocatalytic degradation kinetics of GEM following the pseudo-first-order reaction. Compared to photolysis ($0.0046\ min^{-1}$) without any catalysts, the degradation rate constant increased to $0.0436\ min^{-1}$ in the presence of TiO_2. The photocatalytic degradation efficiencies ($0.0523–0.101\ min^{-1}$) of the TiO_2/C-Dots composites are obviously better than TiO_2 nanoparticles, demonstrating the remarkable effects of the TiO_2/C-Dots composites on the photocatalytic degradation of GEM under simulated sunlight irradiation. The 5.0% C-Dots content in the TiO_2/C-Dots composites seems to be the preferred condition for the photocatalytic degradation of GEM. It is approximately 22 times and 2.3 times faster than degradation by direct photolysis and TiO_2 photocatalytic degradation, respectively. Further increasing the loading amount of C-Dots decreases the GEM degradation efficiency (Table 1), implying that the excess C-Dots play a role in impeding the transformation of photogenerated electrons by surface adsorbed GEM and free radicals. In addition, a high concentration of C-Dots could absorb the emission energy of the C-Dots themselves and lead to lower energy transferred to the TiO_2/C-Dots composites [7]. Therefore, the proper weight percent of C-Dots in the TiO_2/C-Dots composites is an important factor for the photocatalytic degradation of GEM.

The photocatalytic activity of the TiO_2/C-Dots composites was further evaluated for the degradation of GEM in aqueous solution under full wavelength, simulated sunlight and visible light irradiation. Obviously, the TiO_2/C-Dots composites exhibit enhanced photocatalytic activity under the three irradiation conditions. Under full wavelength irradiation, the removal rate of GEM in the presence of the TiO_2/C-Dots composites is approximately 89% at 8.0 min (Fig. 2a). This is 1.26 times and 1.44 times higher than those in the conditions of P25 (70.5%) and prepared TiO_2 (61.8%). As shown in Fig. 2b, the TiO_2/C-Dots composites (58.0%) exhibit higher photocatalytic activity than P25 (31.8%) and pure TiO_2 (28.0%) under simulated sunlight irradiation, indicating that the degradation efficiency of the TiO_2/C-Dots composites is 1.58 times and 2.07 times better than those of P25 and TiO_2, respectively. Under visible light irradiation, the photocatalytic degradation in the presence of the TiO_2/C-Dots composites is still effective with approximately 40% GEM elimination at 8.0 min (Fig. 2c). However, in the presence of P25 and TiO_2, no apparent degradation of GEM is observed. The weaker photocatalytic activity of P25 and TiO_2 can be ascribed to their poor response to light over 420 nm [29]. After C-Dots are assembled onto TiO_2, the TiO_2/C-Dots composites can be utilized under visible light.

As shown in Fig. 1E, the absorption spectrum of the TiO_2/C-Dots composites is extended from the UV region to the visible light region by certain functional groups (C, C—O, C═O and O—H groups) compared with TiO_2. The sensitization of C-Dots enables the redshift of the absorption peak of TiO_2 from 395 nm to 445 nm based on the color changing from the initially pure color to the brown color of the C-Dots suspension (inset from Fig. 1E). Moreover, the upconversion ability of the C-Dots could be converted from a near infrared emission wavelength to visible light (Fig. 1A), which enhances the photocatalytic efficiency of TiO_2 under sun-

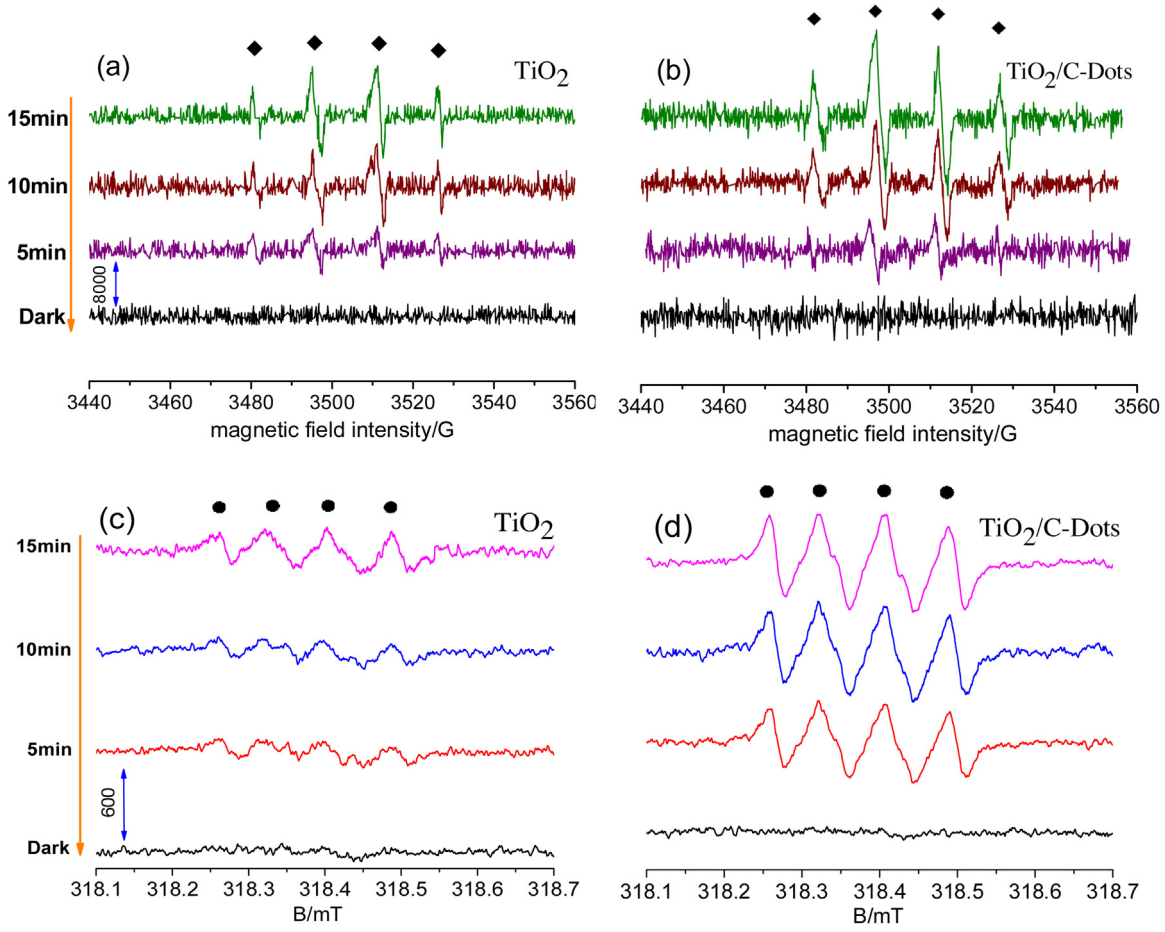

Fig. 3. ESR spectra of the (a and b) DMPO-•OH and (c and d) DMPO—O_2•$^-$ adducts recorded with (a and c) pure TiO_2 and (b and d) 5 wt% TiO_2/C-Dots under simulated sunlight irradiation, [DMPO] = 50 mM; [TiO_2] = 0.05 g l^{-1}, [TiO_2/C-Dots] = 0.05 g l^{-1}; [GEM] = 2 mg l^{-1}; pH = 7.0.

light irradiation [30]. For the analysis of e^- transfer under simulated sunlight irradiation, the high fluorescence intensity of C-Dots produced more photogenerated e^-, in which the photogenerated e^- leap and recombine quickly with hv^+. After modification, fluorescence quenching occurred in the TiO_2/C-Dots composites (Fig. S6). This means that the photogenerated e^- transferred to the conduction band of TiO_2 but did not recombine with hv^+. As the e^- donor, C-Dots can provide lots of e^- to TiO_2 [31]. Thus, e^- transfer between TiO_2 and the C-Dots is likely to improve photocatalytic performance. In addition, the proper photoelectric characteristics, including the lowest unoccupied molecular orbital energy level of C-Dots (4.2–4.4 eV) and the band gap of TiO_2, (3.2 eV) are conducive to the optical e^- transfer from the conduction band of TiO_2 to the interface [32,33]. Zhang et al. [34] reported that the transfer rate of e^- can be effectively enhanced when the hv^+ is left from the TiO_2, followed hv^+ reacted with OH^- to generate •OH (oxidation potential, +2.7 V). The separation of e^- promotes the generation of O_2•$^-$ via the scavenging e^- with adsorbed O_2 on the photocatalyst surface, since the conduction band potential of TiO_2 (0.40 V) is more negative than the standard redox potential E_0 (O_2/O_2•$^-$, −0.33 V). Therefore, the TiO_2/C-Dots composites produce prominent photocatalytic activity in comparison to bare TiO_2.

The photocatalysis cyclic performance by the TiO_2/C-Dots composites under simulated sunlight irradiation was also studied. There is no obvious decrease in photocatalytic degradation activity or change of XRD pattern even after five cycles (Figs. 2d and S7). It can be concluded that the TiO_2/C-Dots composites as catalyst have superior stability and reusability.

3.3. Influence of the major RSs on photocatalytic degradation

RSs generated from the TiO_2/C-Dots composites under simulated sunlight irradiation were probed by a DMPO spin-trapping ESR technique. As shown in Fig. 3, no ESR signal is found in dark conditions, while four-line ESR signals with intensity ratios of 1:2:2:1 and 1:1:1:1are observed under simulated sunlight irradiation. These four-line ESR signals represent the presence of DMPO •OH and DMPO O_2•$^-$ adducts according to a report by Wang et al. [35]. Thus, •OH and O_2•$^-$ were shown to be involved in the photocatalytic degradation process by both of TiO_2 and the TiO_2/C-Dots composites. The intensities of the •OH and O_2•$^-$ signals gradually increased in the presence of TiO_2 and TiO_2/C-Dots composites with the increasing irradiation time from 0 min to 15 min, indicating the important roles of •OH and O_2•$^-$ in removal of GEM [36]. The notably higher formation rates of •OH and O_2•$^-$ are also observed from the TiO_2/C-Dots system than those from the TiO_2. According to the results shown in Fig. 2, the GEM degradation rate is higher in the presence of TiO_2/C-Dots composites than in the presence of TiO_2. This implies that the increased generation of •OH and O_2•$^-$ leads to a higher degradation rate of GEM.

In addition to direct determination of RSs by ESR tests, indirect analysis by the addition of scavengers was also conducted in this study. Four scavengers, potassium iodide (KI), isopropanol, silver nitrate ($AgNO_3$) and 4-hydroxy-2,2,6,6-tetramethylpiperidinyloxy (TEMPL), were used to quench •OH and hv^+, •OH, e^-_{aq}, and O_2•$^-$ in this study [37,38]. The results, including the first order rate constants and the corresponding contribution rates of GEM pho-

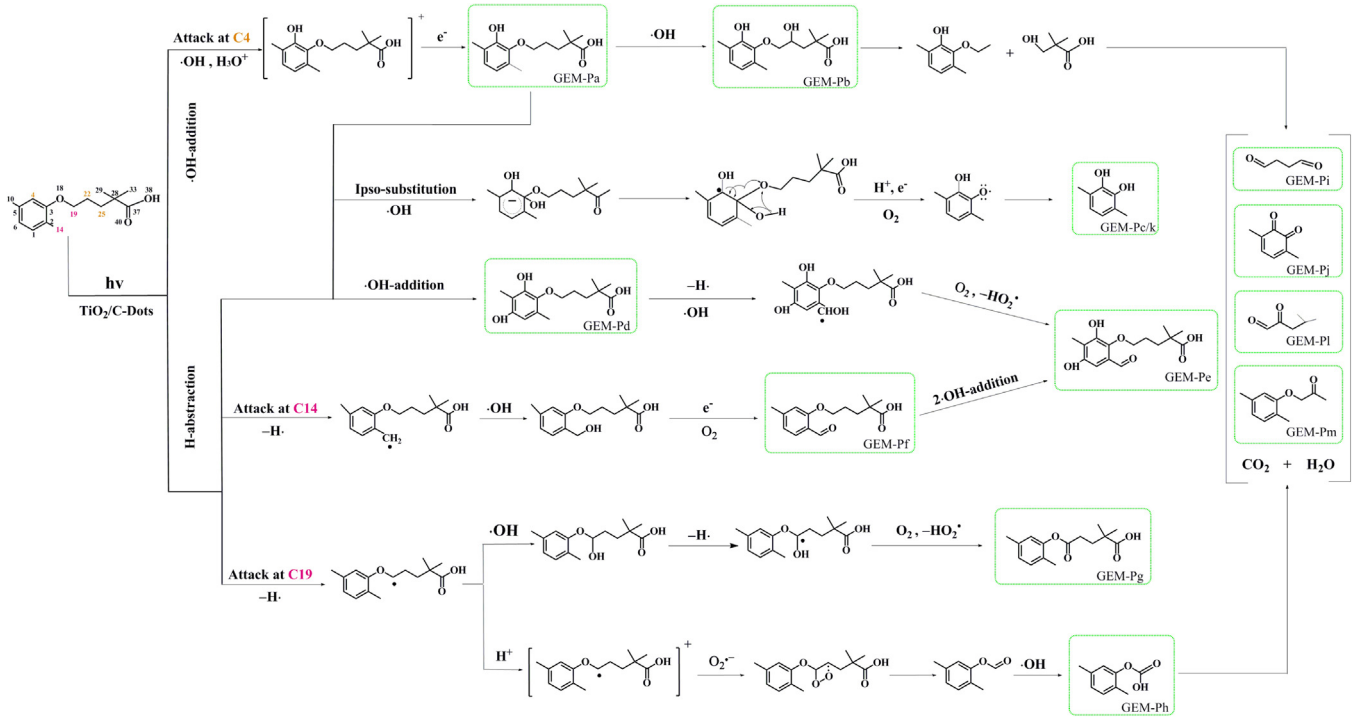

Fig. 4. Proposed photocatalytic degradation pathways of GEM under simulated sunlight irradiation (TiO_2/C-Dots composites (5.0 wt%)).

Table 2
The rate constants for photocatalytic degradation of GEM with the addition of different scavengers, [TiO_2/C-Dots] = 0.05 g l^{-1}.

Photocatalytic conditions	Quenching RSs	Quencher concentration	k(min^{-1})	Contribution rate/%
No scavengers	/	/	0.101 ± 0.004	/
KI	Quench h^+ and HO•	50 mM	$(7.44 \pm 0.24) \times 10^{-3}$	92.6
		100 mM	$(6.14 \pm 0.16) \times 10^{-3}$	93.9
Isopropanol	Quench HO•	50 mM	$(16.0 \pm 0.51) \times 10^{-3}$	84.1
		100 mM	$(15.9 \pm 0.14) \times 10^{-3}$	83.5
$AgNO_3$	Quench e^-_{aq}	20 mM	$(97.0 \pm 0.47) \times 10^{-3}$	3.6
		50 mM	$(97.5 \pm 0.29) \times 10^{-3}$	3.1
TEMPL	Quench $O_2^{\bullet -}$	2 mM	$(85.9 \pm 0.34) \times 10^{-3}$	14.6
		10 mM	$(88.8 \pm 0.35) \times 10^{-3}$	11.7

tocatalysis, in the different conditions are shown in Table 2. The rate constant of the reference condition, which was the absence of any scavengers, is 0.101 min^{-1}. After the addition of KI, the degradation rates of GEM decline sharply by more than 90% due to the quenching of •OH and hv^+. Except for these two RSs, the average contribution rates of e^-_{aq} and $O_2^{\bullet -}$ are 3.4% and 13.2% in the presence of $AgNO_3$ and TEMPOL. Although Razavi et al. [37] have demonstrated that e^-_{aq} reacts with GEM with a high rate constant ($(6.26 \pm 0.58) \times 10^8$ M^{-1} s^{-1}), the contribution of e^-_{aq} is quite low in the present study. This likely can be explained by the production of $O_2^{\bullet -}$ based on the reaction of migration of e^-_{aq} and dissolved oxygen. In addition, the introduction of isopropanol also obviously decreases the average rate constant of GEM photodegradation to 16.0×10^{-3} min^{-1}, indicating that •OH is the main contributor to the degradation of GEM with a high average contribution rate of 83.8%.

Overall, a smaller contribution is associated with indirect degradation of reductive species e^-_{aq} which produces $O_2^{\bullet -}$ at the TiO_2/C-Dots conduction band. Due to the insolubility in aqueous solution, the hydrophobic substances are favorable to reacting with hv^+, leading to adsorption on the surface of the photocatalyst [39]. However, GEM is hydrophilic so hv^+ may not play a substantial role in the degradation of GEM. The results of direct and indirect determination suggested that •OH is the most important RSs during the photocatalytic process. To our knowledge, •OH is a highly electrophilic substance that preferentially attacks at activated (i.e., electron-dense) sites of aromatic rings. This further demonstrates that GEM is easily degraded by •OH on account of the rich electronic system of the methyls, which is supported by our previous studies about the •OH-induced degradation of mefenamic acid [40].

3.4. Photocatalytic degradation mechanism

3.4.1. Identification of photocatalytic degradation by-products

As shown in Figs. S8 and S10, thirteen peaks of major degradation by-products detected by HPLC/MS/MS and GC/MS are assigned from GEM-Pa to GEM-Pm, and the structures and relative parameters are elaborated in Table S2, Fig. S9, Table S3 and Fig. S11.

The retention times of the by-products were lower than that of GEM, suggesting that the by-products are more hydrophilic than their parent compound. Among these intermediates, GEM-Pc/k and Ph-Pm appear to be the by-products of ether chain cleavage. The ipso-directed oxidation of GEM results in the formation of by-products with the molecular weight (MW) of 138.

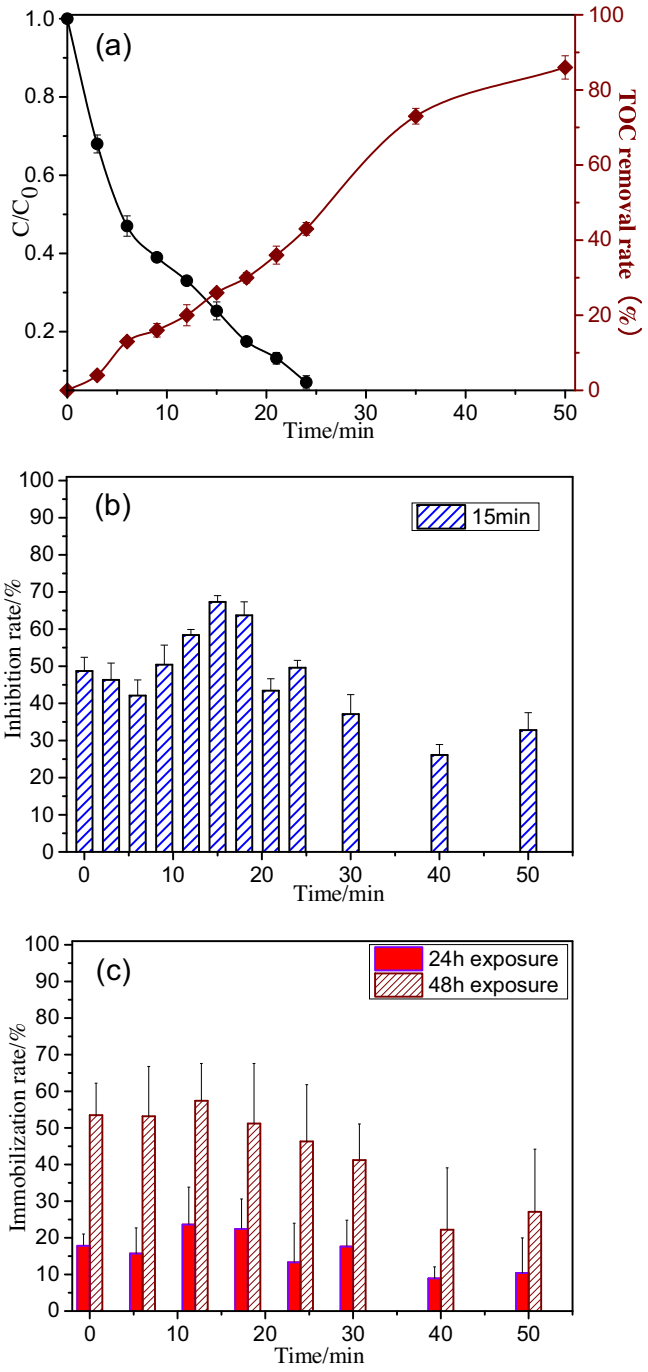

Fig. 5. (a) Evolution of both TOC removal efficiencies (brown curve, right y-axis) and GEM degradation rate (black curve, left y-axis) during the photocatalytic degradation of 2 mg l^{-1} GEM by 0.05 g l^{-1} TiO_2/C-Dots composites (5 wt%); Acute toxicity evaluated by (b) *V. fischeri* for 15 min, (c) *D. magna* for 24 h and 48 h exposure times.

GEM-Pa and GEM-Pf should be the isomers due to the same molecular weight. They originated from the addition of 16 amu to the mono-hydroxylated GEM (•OH addition to the benzene ring) and acetalization. Assignment of these intermediates is further supported by the study of ^{137}Cs γ-irradiation and photolysis mediated GEM degradation [37,41,42]. The addition of •OH to the benzene ring of GEM-Pa and Pf also lead to the formation of by-products with MW 282 (GEM-Pb and Pd) and MW 296 (GEM-Pe). Intermediate *m*/*z* 264 was identified to be 2,2-dimethyl-pentanedioic acid 5-(2, 5-dimethyl-phenyl) ester based on the ketonization of by-product (250 *m*/*z*) with an addition of 14 amu (Fig. 4).

3.4.2. Theoretical calculation and degradation pathways

According to the atomic model of GEM (Fig. S12), the FEDs and point charge of GEM was calculated to predict the reaction positions for •OH and $O_2^{\bullet-}$ attack using the Frontier Orbital Theory (Table 3). Positions with relatively higher values of FED^2_{HOMO}+ FED^2_{LUMO} are considered more susceptible to •OH attack [25]. It can be observed that C4 (1.8433), C22 (3.5742) and C25 (1.9924) atoms have higher values of FED^2_{HOMO}+ FED^2_{LUMO} than other atoms, indicating that these three reaction sites are likely to be attacked by •OH through the pathways of •OH addition. Due to its non-selectivity, •OH was added to the GEM structure with molar ratios from 1:1 to 1:3. When the •OH addition attacked at C4, C22 or C25 atoms, the transient states of the •OH adduct radicals were formed, resulting in the formation of the hydroxylated by-products (e.g., GEM-Pa), followed by further radical oxidation to form stable by-products (GEM-Pb and Pd). When the •OH addition reaction took place on the ipso aromatic C atom of GEM-Pa, this ipso-substitution led to stabilized carbon-centered radicals [43]. In addition, O-dealkylation reactions caused either side chain cleavage of the parent compound, giving rise to the generation of GEM-Pc/k. GEM-Pc/k has been detected by ^{137}Cs γ-irradiation in a previous study [37].

Another reaction pathway is H-abstraction. Based on the theory that electron withdrawing groups can weaken the stability of the transition state, H-abstraction reactions considerable affect the formation of degradation by-products. The H-abstraction reaction generally takes place in atoms with a higher positive charge. As shown in Table 3, C14 (0.1192) and C19 (0.7447) possess higher positive charge values compared with other atoms. Therefore, the H abstraction reaction occurred at C14 and C19 atoms, resulting in the formation of a GEM free radical. The addition of O_2 to the radical and the elimination of HO_2• then produced GEM-Pg and Pf. Then, these by-products were oxidized by •OH and transformed to a hydroxylated benzaldehyde derivative (GEM-Pe) [43].

In plenty of heterogeneous photocatalytic reactions, dissolved oxygen has been found to affect the generation of degradation by-products [44]. It serves as a trap for the photocatalysis-generated conduction electron and mediates the formation of nucleophilic $O_2^{\bullet-}$, which is suggested to preferentially interact with GEM^+ at reaction positions with a higher positive point charge to form a zwitterion or a diradical [45,46]. In addition, a supporting mechanism proposed by Wahab et al. [43] may be expected for $O_2^{\bullet-}$ attack. Thus, the trapping of GEM by $O_2^{\bullet-}$ was speculated to occur at C19 to generate GEM-Ph. Finally, GEM and its formed by-products could be further completely mineralized into CO_2 and H_2O by prolonging the irradiation time (Fig. 5a).

In summary, the results of LC/MS/MS and GC/MS analyses, as well as the proposed pathways illustrate the significant roles of •OH and $O_2^{\bullet-}$ over the reaction with GEM. According to the deduced byproducts (such as GEM-Pa, Pb, Pc, Pd and Pe), the primary mechanism has been confirmed that •OH is the main radicals in the photocatalytic degradation of GEM. This finding is in accordance with above results of ESR analyses and quenching experiments.

3.5. Ecotoxicity of treated solutions and transformation by-products

Two organisms with different trophic levels, including *V. fischeri* and *D. magna*, were used to evaluate the change of toxicity during the photocatalytic degradation process. The initial inhibition rate of GEM by *V. fischeri* was 48.7% at 15 min exposure time, while the original immobilization rate of *D. magna* was 17.8% and 53.5% at 24 h and 48 h duration time, respectively. Initially, the inhibition efficiencies decreased because the degradation was primarily by GEM itself and lacking the accumulation of by-products. As shown in Fig. 5b and c, the inhibition rate by *V. fischeri* and the immobilization rate by *D. magna* reached the maximum values observed

Table 3
FEDs on atoms of GEM calculated using the Gaussian 09 program at the b3lyp/6-311+g (d, p).

Atom(number)[a]	$2FED^2_{HOMO}$	$FED^2_{HOMO} + FED^2_{LUMO}$	Point charge	Atom (number)[a]	$2FED^2_{HOMO}$	$FED^2_{HOMO} + FED^2_{LUMO}$	Point charge
1C	0.0038	0.5504	0.0646	*19C*[b]	0.01333	0.4930	*0.7447*
2C	0.3082	0.8177	−0.0969	**22C**	0.0160	**3.5742**	0.0948
3C	0.2031	0.5348	0.8128	**25C**	0.0469	**1.9924**	0.0921
4C	0.0630	**1.8433**	−0.2807	28C	0.0533	0.2182	0.0553
5C	0.1077	0.7283	0.1984	29C	0.0010	0.0100	0.0413
6C	0.2141	0.6288	−0.2449	33C	0.0025	0.2633	0.0409
10C	0.0089	0.1126	0.0905	37C	0.0005	0.0455	1.4548
14C	0.0147	0.1252	*0.1192*	38O	0.0001	0.0033	−0.9259
18O	0.2317	0.1202	−1.2397	40O	0.00003	0.0029	−0.9982

[a] See Fig. S12 for atom numbering.
[b] The values denote the big ones for •OH-addition (bold font) and H-abstraction (italic font).

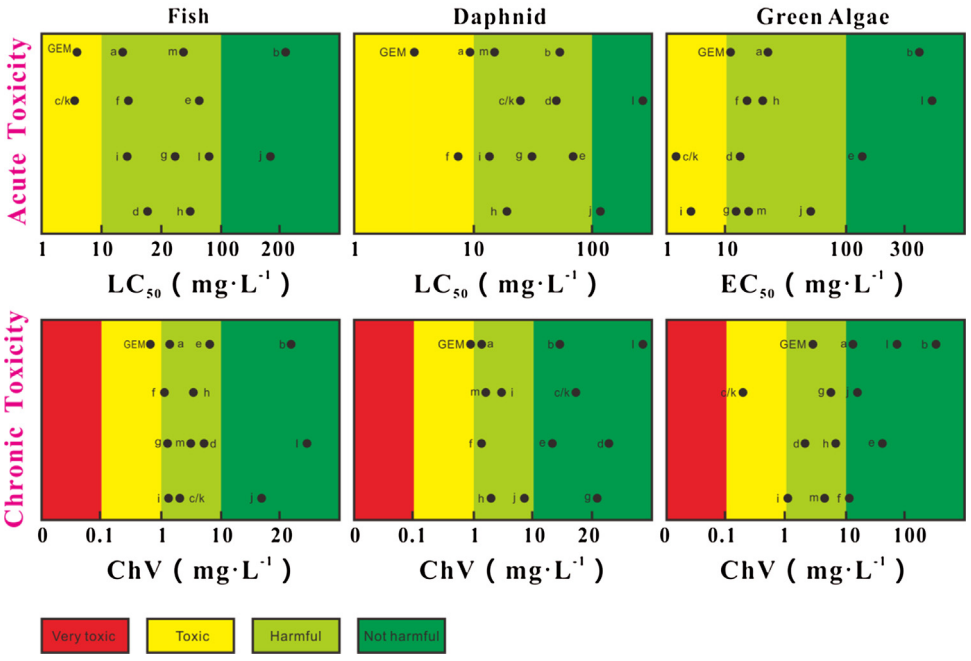

Fig. 6. Evolution of acute and chronic toxicities and toxicity classification for GEM and its transformation by-products GEM-Pa-Pm.

in the treated solution at 15 min (67.3%) and 12 min (23.6% and 57.4%). At the irradiation time of 12–18 min, the transformation rate of GEM was in the range of 67.0–82.5%, whereas only ~30% of the TOC removal rate was achieved. Therefore, the higher toxicity in the treated solution than in the initial GEM solution at this time interval is from the residue degradation by-products due to incomplete mineralization (Fig. 5a). A similar result was also reported by Méndez-Arriaga et al. [47] for the treatment of propylparaben by TiO_2 photocatalytic technology. The toxicity to *V. fischeri* and *D. magna* decreased from 20 min to 50 min with the increasing TOC removal rate, indicating the elimination of high toxic intermediates.

To further assess the toxicity of transformation by-products, the acute toxicity (LC_{50} or EC_{50}) and chronic toxicity of these by-products were calculated by ECOSAR software [48,49]. The predicted values of GEM and its transformation by-products in the neutral form are given in Table S4. The Daphnia was the most sensitive species for GEM, and the predicted acute toxicities towards Daphnia for all the identified by-products in this study were lower than that of GEM itself. Except for the predicted LC_{50} to fish of GEM-Pc/k and EC_{50} to green algae of GEM-Pc/k and Pi, the predicted values of by-products towards fish and green algae were higher than those of GEM. The chronic toxicity was similar to the acute toxicity in that the predicted toxicity values for most by-products are lower than GEM. According to the EU Directive No. 67/548/EEC and the Chinese hazard evaluation guidelines for new chemical substances (HJ/T 154e2004), GEM and its transformation by-products are classified to different toxic levels (Fig. 6). Previous studies have shown that GEM can be degraded by some techniques, such as chlorination, microbial degradation and ^{137}Cs γ-irradiation [37,50,51]. However, a considerable number of their transformation by-products (e.g., halogenated by-products, chroman products and ketonized by-products) present more toxicity to aquatic organisms in comparison to GEM itself (Table S5). For instance, the toxicity of Pγb, which is a cyclohexa compound, exhibits toxicity at least one order of magnitude higher than other by-products. In contrast, the toxic levels of most by-products show one or two orders of magnitude lower than GEM by TiO_2/C-Dots photocatalytic technology. This can be attributed to the environmentally friendly mechanism of the present technology for example the •OH-induced photocatalytic degradation. Thus, as a promising alternative to conventional water treatment technology, TiO_2/C-Dots photocatalytic technology performs excellently in reducing the acute eco-toxicity of treated solutions and the generation of toxic by-products of GEM.

4. Conclusion

The photocatalytic activity of the TiO_2/C-Dots composites in GEM degradation was 2.1 and 3.3 times better than the bare TiO_2 under simulated sunlight irradiation and visible light irradiation, respectively. The results of ESR, HPLC/MS/MS and GC/MS

demonstrate the participation of •OH and $O_2^{\bullet-}$ in the degradation of GEM. Based on the identification of by-products and the calculation of frontier electron density, •OH addition, H abstraction and $O_2^{\bullet-}$ attack are proposed to be the major RSs-mediated pathways. During the photocatalytic process, the changes of toxicity to two aquatic organisms initially reached a maximum value, and finally decreased with the increasing TOC removal rate. This photocatalytic technique could reduce the generation of toxic by-products compared with other traditional AOPs via the prediction of ECOSAR. To our knowledge, it is the first time TiO_2/C-Dots photocatalytic activity was evaluated through investigating the degradation mechanism of PPCPs. This study presents a promising sunlight-driven photocatalyst for practical applications in the treatment of drinking water and wastewater.

Acknowledgments

This work was supported by National Natural Science Foundation of China (No. 21377031 and 21677040), the Innovative Team Program of High Education of Guangdong Province (2015KCXTD007).

Appendix A. Supplementary data

Supplementary data associated with this article can be found, in the online version, at http://dx.doi.org/10.1016/j.apcatb.2016.11.040.

References

[1] J.L. Zhao, G.G. Ying, Y.S. Liu, F. Chen, J.F. Yang, L. Wang, X.B. Yang, J.L. Stauber, M.S.J. Warne, Environ. Toxicol. Chem. 29 (2010) 1377–1384.
[2] Y. Fang, A. Karnjanapiboonwong, D.A. Chase, J. Wang, A.N. Morse, T.A. Anderson, Environ. Toxicol. Chem. 31 (2012) 550–555.
[3] L. Lishman, S.A. Smyth, K. Sarafin, S. Kleywegt, J. Toito, T. Peart, B. Lee, M. Servos, M. Beland, P. Seto, Sci. Total Environ. 367 (2006) 544–558.
[4] P. Pocostales, P. Álvarez, F.J. Beltrán, Chem. Eng. J. 168 (2011) 1289–1295.
[5] L. Qin, Y.L. Lin, B. Xu, C.Y. Hu, F.X. Tian, T.Y. Zhang, W.Q. Zhu, H. Huang, N.Y. Gao, Water Res. 65 (2014) 271–281.
[6] R. Liang, S. Luo, F. Jing, L. Shen, Q. Na, W. Ling, Appl. Catal. B: Environ. 176 (2015) 240–248.
[7] R. Miao, Z. Luo, W. Zhong, S.Y. Chen, T. Jiang, B. Dutta, Y. Nasr, Y. Zhang, S.L. Suib, Appl. Catal. B: Environ. 189 (2016) 26–38.
[8] Z. Hui, L. Zhao, F. Geng, L.H. Guo, B. Wan, Y. Yu, Appl. Catal. B: Environ. 180 (2016) 656–662.
[9] K. Nakata, A. Fujishima, J. Photochem. Photobiol. C: Photochem. Rev. 13 (2012) 169–189.
[10] X. Yang, J. Qin, Y. Li, R. Zhang, H. Tang, J. Hazard. Mater. 261 (2013) 342–350.
[11] J. Tian, Y. Leng, Z. Zhao, Y. Xia, Y. Sang, P. Hao, J. Zhan, M. Li, H. Liu, Nano Energy 11 (2014) 419–427.
[12] X. Yang, J. Qin, J. Yan, K. Chen, X. Yan, Z. Du, L. Rong, T. Hua, Appl. Catal. B: Environ. 166–167 (2015) 231–240.
[13] X. Yang, J. Qin, Y. Jiang, R. Li, Y. Li, H. Tang, RSC Adv. 4 (2014) 18627–18636.
[14] C. Cheng, X. Tan, D. Lu, L. Wang, T. Sen, J. Lei, A.M. El-Toni, J. Zhang, F. Zhang, D. Zhao, Chem. Eur. J. 21 (2015) 17944–17950.
[15] J. Xia, J. Di, H. Li, X. Hui, H. Li, S. Guo, Appl. Catal. B: Environ. 181 (2016) 260–269.
[16] H. Li, X. Zhang, D.R. Macfarlane, Adv. Energy Mater. 5 (2015), http://dx.doi.org/10.1002/aenm.201401077.
[17] L. Feng, H. Sun, J. Ren, X. Qu, Nanotechnology 27 (2016) 569–579.
[18] Y. Zhang, C.W. Foster, C.E. Banks, L.D. Shao, H.S. Hou, G.Q. Zou, J. Chen, Z.D. Huang, X.B. Ji, Adv. Mater. 28 (2016) 9391–9399.
[19] H. Li, X. He, Y. Liu, H. Yu, Z. Kang, S.T. Lee, Mater. Res. Bull. 46 (2011) 147–151.
[20] F. Wang, Y. Zhang, Y. Liu, X. Wang, M. Shen, S.T. Lee, Z. Kang, Nanoscale 5 (2013) 1831–1835.
[21] X. Han, Y. Han, H. Huang, H. Zhang, X. Zhang, R. Liu, Y. Liu, Z. Kang, Dalton Trans. 42 (2013) 10380–10383.
[22] K. Li, F.Y. Su, W.D. Zhang, Appl. Surf. Sci. 375 (2016) 110–117.
[23] M. Sun, X. Ma, X. Chen, Y. Sun, X. Cui, Y. Lin, RSC Adv. 4 (2014) 1120–1127.
[24] M.E. Casas, R.K. Chhetri, G. Ooi, K.M.S. Hansen, K. Litty, M. Christensson, C. Kragelund, H.R. Andersen, B. Kai, Water Res. 83 (2015) 293–302.
[25] T. An, G. Li, W. Song, J. An, Y. Gao, H. Fang, Appl. Catal. B: Environ. 164 (2015) 279–287.
[26] S. Qu, X. Wang, Q. Lu, X. Liu, L. Wang, Angew. Chem. 51 (2012) 12381–12384 (12384).
[27] OECD, Guideline for Testing of Chemicals 202: Daphnia Sp. Acute Immobilization Test and Reproduction Test, OECD, Paris, 1981.
[28] ECOSAR, http://www.epa.gov/oppt/newchems/tools/21ecosar.htm, 2013.
[29] Z. Lei, L. Zhao, Y. Jin, M. Li, W. Song, C. Xie, Appl. Catal. B: Environ. 166–167 (2015) 1–8.
[30] Y. Han, H. Huang, H. Zhang, Y. Liu, X. Han, R. Liu, H. Li, Z. Kang, ACS Catal. 4 (2014) 1367–1370.
[31] H. Zhang, H. Huang, H. Ming, H. Li, L. Zhang, Y. Liu, Z. Kang, J. Mater. Chem. 22 (2012) 10501–10506.
[32] Y. Li, B.P. Zhang, J.X. Zhao, Z.H. Ge, X.K. Zhao, L. Zou, Appl. Surf. Sci. 279 (2013) 367–373.
[33] H. Zheng, T. Zhai, M. Yu, S. Xie, C. Liang, W. Zhao, S.C.I. Wang, Z. Zhang, X. Lu, J. Mater. Chem. C 1 (2012) 225–229.
[34] Y.Q. Zhang, D.K. Ma, Y.G. Zhang, W. Chen, S.M. Huang, Nano Energy 2 (2013) 545–552.
[35] H. Wang, Y. Su, H. Zhao, H. Yu, S. Chen, Y. Zhang, X. Quan, Environ. Sci. Technol. 48 (2014) 11984–11990.
[36] D. Dvoranová, Z. Barbieriková, V. Brezová, Molecules 19 (2014) 17279–17304.
[37] B. Razavi, W. Song, W.J. Cooper, J. Greaves, J. Jeong, J. Phys. Chem. A 113 (2009) 1287–1294.
[38] G. Li, N. Xin, J. Chen, J. Qi, T. An, P.K. Wong, H. Zhang, H. Zhao, H. Yamashita, Water Res. 86 (2015) 17–24.
[39] E. Hapeshi, A. Achilleos, M.I. Vasquez, C. Michael, N.P. Xekoukoulotakis, D. Mantzavinos, D. Kassinos, Water Res. 44 (2010) 1737–1746.
[40] P. Chen, W. Lv, Z. Chen, J. Ma, R. Li, K. Yao, G. Liu, F. Li, Environ. Sci. Pollut. Res. Int. 22 (2015) 12585–12596.
[41] M. Cermola, M. Dellagreca, M.R. Iesce, L. Previtera, M. Rubino, F. Temussi, M. Brigante, Environ. Chem. Lett. 3 (2005) 43–47.
[42] J. Ma, W. Lv, C. Ping, Y. Lu, F. Wang, F. Li, K. Yao, G. Liu, Environ. Sci. Pollut. Res. (2016) 1–13.
[43] W. Song, W.J. Cooper, S.P. Mezyk, J. Greaves, B.M. Peake, Environ. Sci. Technol. 42 (2008) 1256–1261.
[44] H.S. Wahab, T. Bredow, S.M. Aliwi, Surf. Sci. 603 (2009) 664–669.
[45] M.N. Möller, D.M. Hatch, H.Y.H. Kim, N.A. Porter, J. Am. Chem. Soc. 134 (2012) 16773–16780.
[46] L. Yin, Z. Shen, J. Niu, J. Chen, Y. Duan, Environ. Sci. Technol. 44 (2010) 9117–9122.
[47] F. Méndez-Arriaga, S. Esplugas, J. Giménez, Water Res. 42 (2008) 585–594.
[48] J. Kuang, J. Huang, B. Wang, Q. Cao, S. Deng, G. Yu, Water Res. 47 (2013) 2863–2872.
[49] R. Zhang, Y. Yang, C.H. Huang, L. Na, L. Hang, Z. Lin, P. Sun, Environ. Sci. Technol. 50 (2016) 2573–2583.
[50] D.N. Bulloch, R. Lavado, K.L. Forsgren, S. Beni, D. Schlenk, C.K. Larive, Environ. Sci. Technol. 46 (2012) 5583–5589.
[51] H. Kjeldal, N.A. Zhou, D. Wissenbach, B.M. Von, H.L. Gough, J. Nielsen, Environ. Sci. Technol. 50 (2015) 744–755.